The drainage of a thin aqueous film between a solid surface and an approaching gas bubble

Leonard R. Fisher[1,a], Emma E. Mitchell[a], David Hewitt[b], John Ralston[b], and Joe Wolfe[c]

[a]*CSIRO Division of Food Processing, P.O. Box 52, North Ryde, N.S.W. 2113 (Australia)*
[b]*School of Chemical Technology, South Australian Institute of Technology, The Levels, P.O. Box 1, Ingle Farm, S.A. 5089 (Australia)*
[c]*School of Physics, University of New South Wales, P.O. Box 1, Kensington, N.S.W. 2033 (Australia)*

Abstract

A new optical technique is used to measure the time-dependent shape of thin aqueous draining films between air bubbles and hydrophilic or hydrophobic quartz surfaces. The thickness is determined to a precision of ± 0.2 nm to ± 1 nm from the intensity of the reflected interference beam from a spot of laser light which is focussed on the thinning film and which is scanned radially. The film shape begins as a dimple which then flattens as it thins. Plots of the thickness as a function of time and of radial position are presented for films of pure water and of 0.23 mol m^{-3} NaCl solution at hydrophilic quartz surfaces. In the ring of closest approach, the pure water film is at all times thicker than that of the salt solution film. In the early phase of the approach, the pure water film thins more slowly at the centre, but after about 40 s it thins more rapidly. Both of these observations are consistent with the expected shorter range of the double layer repulsion in the salt solution. For hydrophobic surfaces, the drainage rate is more rapid, the film eventually collapsing.

INTRODUCTION

The approach to a solid surface of a gas bubble in a liquid is central to the process of mineral flotation [1]. It is also an example of the draining of a thin liquid film between two other phases, a process which determines the behaviour of many colloidal suspensions [2,3].

Figure 1 (inset) shows the typical shape of a film trapped between an air bubble and a solid surface. For a thin, axisymmetric film the liquid flow is

---

[1]Present address: Department of Anatomy and Developmental Biology, University College London, Gower Street, London WC1E 6BT, United Kingdom.
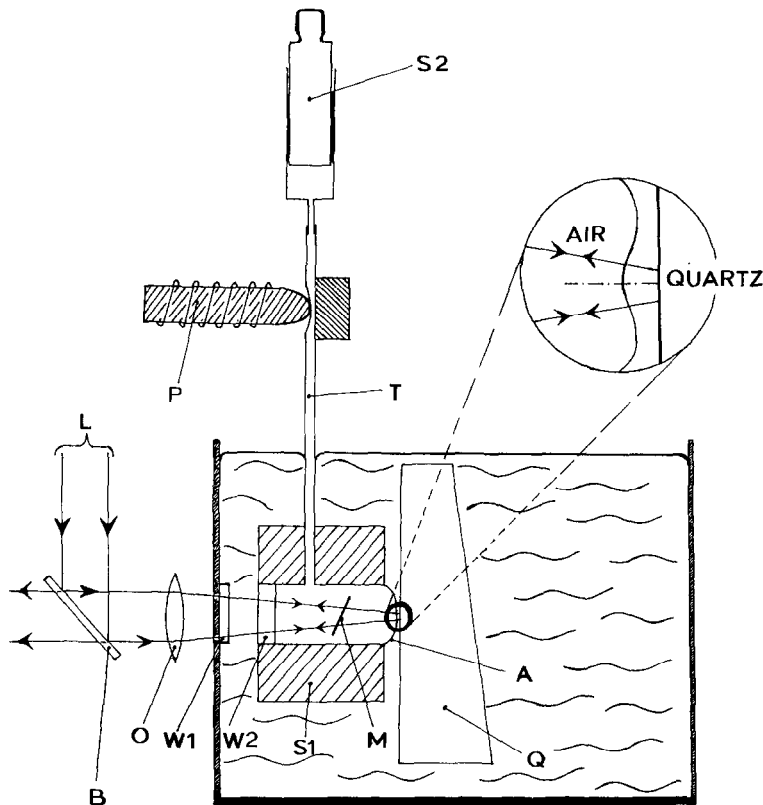
Fig. 1. Median vertical section (schematic) of apparatus. A vertically polarised laser beam L is directed via a polarising beamsplitter B through an objective lens O. After passing through windows W1 (chamber) and W2 (septum) the beam enters an air-filled Perspex (R) septum S1, fed by a micrometer-driven syringe S2 via a silastic tube T. The beam passes through a mica quarter wave plate M (angled to prevent unwanted reflections) and is focussed at the front face of an optically polished quartz prism Q. The air bubble A, initially just out of contact with the quartz surface, is bulged rapidly by allowing a spring-loaded plunger to rapidly compress a section of the silastic tubing. The draining film assumes a "dimpled" configuration within 0.5 s of bubble expansion (inset). The reflected laser beam again passes through the quarter-wave plate, so becoming horizontally polarised and able to pass through the beam splitter and enter a detecting photomultiplier (not shown). Reflections from the windows are, however, eliminated, since the light is vertically polarised. A particular advantage of the optical arrangement is that the beamsplitter and objective (mounted on the micrometer driven carriage) can be moved laterally, so that the beam can be scanned across the film.

approximately radial and the pressure P in the film is a function only of time t and of r_1, the distance from the axis of symmetry. P has three components:

$$P = -\gamma C - F + P_b \qquad (1)$$

The surface tension γ multiplied by the local curvature C is the capillary pres-

sure. F is the force per unit area exerted between the two interfaces and includes electric, van der Waals and other interactions. At close approach this term is large and dominates the behaviour of very thin films. The dependence of F on film thickness is determined by the nature of the surface and by the electrolyte concentration in the aqueous phase. The pressure P_b in the bubble is constant for a stationary bubble of fixed size. Both are important in mineral flotation, the nature of the surface being particularly important, since the draining film can eventually rupture at a hydrophobic surface, producing bubble attachment and hence allowing separation of hydrophobic (desired) mineral particles from hydrophilic (unwanted) particles such as quartz.

Gradients in the film pressure P drive viscous flow (the inertia of the liquid is negligible). The equations for viscous flow and for continuity lead to a complicated differential equation relating the thickness h to radius r and time t. A derivation of this equation is given in Appendix 1.

It has long been known [4,5] that the draining film may have a reverse curvature — the thickness may have a local maximum on the axis of symmetry. This can be qualitatively explained thus: the fluid in the (initially thick) outer regions is close to the bulk and so its drainage is opposed by only a small viscous drag. More rapid draining at the edge than at the centre eventually forms a convex "dimpled" shape (Fig. 1). The convex shape produces a positive Laplace pressure in the centre, and it is this pressure which drives the drainage of the liquid trapped in the centre.

Drainage rates and the shape of the film depend strongly on the initial approach of the bubble to the surface. (Similarly, solutions to the equation describing the system depend on the initial conditions.) For this reason, particular attention must be paid to reproducing initial conditions in any experimental investigation of the effect of solution and surface parameters on the behaviour of the film.

We report here such a series of experiments which show the effects of surface hydrophobicity and solution electrolyte concentration on the time evaluation of the profiles of draining aqueous films between an air bubble and an optically flat quartz surface.

EXPERIMENTAL

The most common way of using optical interferometry to measure thin film profiles is to illuminate the film with a parallel, monochromatic light beam so as to produce a set of interference fringes (Newton's rings if the film is axisymmetric) whose spacing and intensity give the profile [6–8]. The disadvantage of this approach is that the accuracy of intensity measurement, and hence the accuracy of the calculated film thickness, is limited [6].

More accurate thickness measurements can be made if the incident beam is focussed onto a small area of the draining film and the intensity of the reflected

beam from this area measured as a function of time. In this approach the film is treated as a Fizeau interferometer [7]. By taking measurements at different distances from the centre of an axisymmetric draining film, the evolution of the film profile with time can be derived.

In our experimental realisation of this second approach [7,9–11], an intensity-stabilized, polarised 2 mW He/Ne laser beam is used as the light source. The optical arrangement is such that normal incidence illumination can be used (Fig. 1) without problems of reflection from windows and other optical components. The diameter of the focussed laser beam in the plane of the draining film is ca 30 μm, calculated from the focal length of the lens (26 mm) and the Rayleigh criterion [12].

A draining film is formed between an air bubble and a quartz surface in the following way. An air bubble is first bulged from a hole (2 mm diameter) in a Kel-F chamber (Fig. 1) to an apical height of 0.57 mm; hence, a radius of 1.16 mm. In addition to the axial optical system, the bubble is also viewed side-on through a camera by transmitted light, and its apex is placed close to the quartz surface (ca 40 μm). After optical alignment to ensure that the quartz/water interface is at the focal plane of the objective lens and normal to the optical axis of the laser beam, and that the reflected beams from the quartz/water and water/air interfaces are coincident with the optical axis, an experiment is begun by activating a spring-loaded lever to rapidly compress a section of the air line supplying the bubble (Fig. 1). Reproducibility of this step was found to be crucial for reproducibility of the subsequent drainage behaviour, as expected from the form of the differential equation describing the drainage (Ref. [13] and Appendix 1). Bubble expansion flattens the bubble at the apex to produce a draining film with a radius of 0.32 ± 0.005 mm (Fig. 1).

The quartz surfaces were optically polished (to 0.1 wavelengths) with the rear surface at 30° to the front so that light reflected from the rear surface was deflected from the light measurement system. For experiments with hydrophilic quartz surfaces, the quartz was prepared by placing it in hot sodium hydroxide solution (3 kmol m^{-3} for 10 s) after which it was thoroughly rinsed in doubly distilled water [14]. The treated surfaces were judged hydrophilic according to the "steam test" [14] and aqueous films formed between air bubbles and these surfaces were stable for up to 3 h, the maximum time of observation.

For experiments with hydrophobic quartz surfaces, a hydrophilic quartz plate was heated for 6–12 h at 160°C, giving a surface with a contact angle for water of 10–20°, depending on the time of treatment. These surfaces were used immediately, the receding contact angle being measured from photographs taken after draining film collapse allowed bubble attachment.

RESULTS AND DISCUSSION

An example of the time dependence of reflected intensity from the draining film centre is given in Fig. 2. Before the bubble expansion there are large,
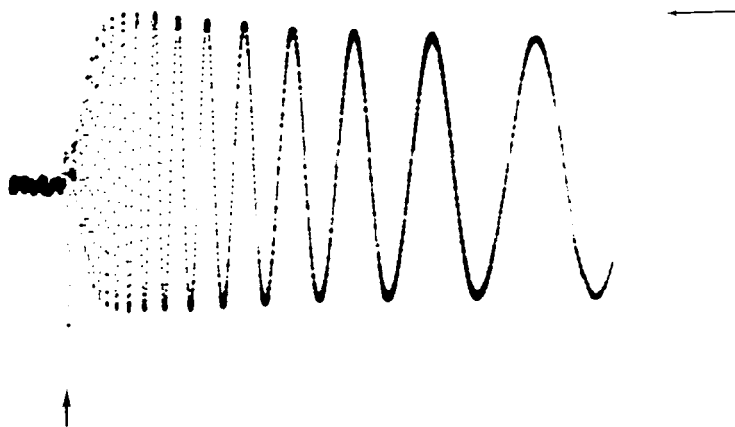
Fig. 2. Reflected beam intensity as a function of time at the centre of a pure water draining film. The difference between successive maxima and minima corresponds to a change in film thickness of 118 nm [11]. The maximum in fringe amplitude at $t = 0.5$ s corresponds to the transition from a convex to a concave (dimpled) air/water interface. Vertical arrow, $t = 0$; horizontal arrow, maximum possible intensity (planar film); total scan time, 10 s.

random fluctuations in the reflected beam intensity caused by thermal movements of the bubble surface. During and following the expansion, a series of interference maxima and minima appear as the aqueous film thins. By interpolating these fringes, the intensity at any time can be used to calculate film thickness with a precision of ± 0.3 to ± 5 nm, depending on whether the intensity is near the average value or near a maximum or minimum in intensity [7,11].

The variation in interference fringe intensity is due to film thickness variations (because of the dimple) across the diameter of the focussed laser beam. The intensity is maximal when the film is flat. Thus the early rapid increase in fringe intensity can be used to obtain information about the thickness and curvature of the film during the establishment of the thin film and the reversal of curvature. We concentrate here, however, on the evolution of the film profile once the dimple is established.

Drainage at a hydrophilic quartz surface

We report here results of experiments using two different compositions of the aqueous phase: pure water in equilibrium with atmospheric gases (conductivity $1.2 \cdot 10^{-4}$ S m^{-1}; surfactant free by the bubble test [14]) and a solution of 0.23 mol m^{-3} sodium chloride. Interference fringes such as those shown in Fig. 2 were used to calculate the thickness of the draining film as a function of time. Results for thinning at the centre and at the radius where the film is thinnest (the barrier ring) are shown in Fig. 3.
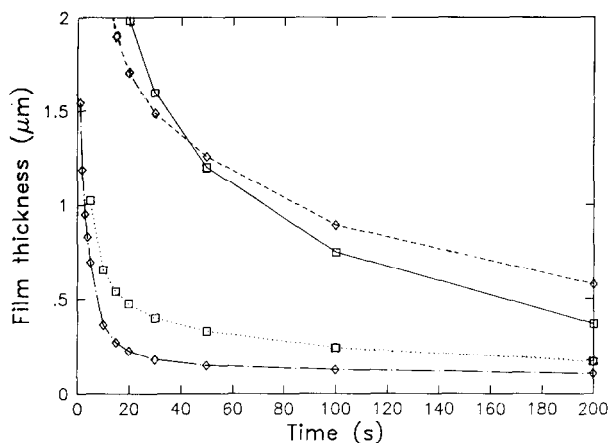
Fig. 3. Aqueous film thickness as a function of time at the centre (upper two curves) and boundary ring (lower two curves) of a dimpled film between an air bubble and a hydrophilic quartz surface. ($\square$) Doubly distilled water; conductivity, $1.2 \cdot 10^{-4}$ S m^{-1}; ($\Diamond$) sodium chloride solution, 0.23 mol m^{-3}.

These data show that the rate of thinning becomes small and slowly varying much earlier in the barrier ring than at the centre, in agreement with the results of other workers [6,15]. The thickness at the centre, on the other hand, remains large rather longer in a film of salt solution. This is consistent with the relatively slow viscous efflux of salt solution through the thin barrier ring.

Data for thinning at various distances from the centre are combined in Fig. 4 to yield the profiles of the pure water film at different times. Similar data (not shown) were obtained for solutions of 0.51 and 0.23 mol m^{-3} sodium chloride solution. The points at each radius come from different experiments, during which the position of the focussed beam was constant. For this reason, small variations in the starting conditions between experiments can give rise to the systematic irregularities in $h(r)$ (Fig. 4). Each of the individual thinning curves (such as those in Fig. 3), though, provide $h(t)$ with accuracy limited only by the interferometry and so yield a more accurate measure of thinning rate as a function of time and/or film thickness at different radii r.

Drainage at hydrophobic surfaces

Quartz plates with contact angles of $10 \pm 5°$ and $20 \pm 3°$ were used for the experiments reported here. Figure 5 shows the rate of thinning as a function of time for pure water films on both hydrophilic and hydrophobic quartz surfaces. Rates of thinning, rather than absolute thickness, are reported for a technical reason: on hydrophilic surfaces a stable film is formed whose thick-
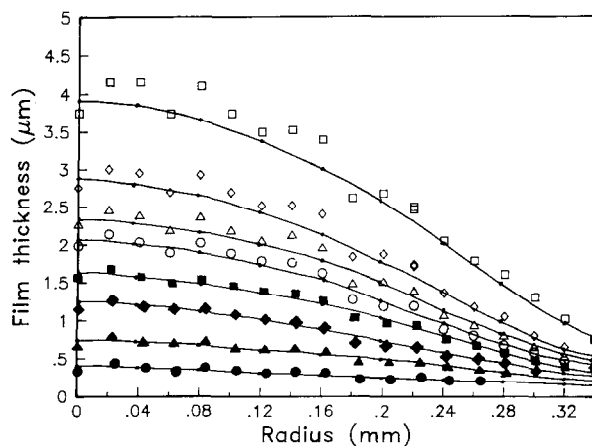
Fig. 4. Film thickness as function of radial distance from the centre (condition as in Fig. 3; conductivity, $1.2 \cdot 10^{-4}$ S m^{-1}). Time from formation of film: ($\square$) 5; ($\diamond$) 10; ($\triangle$) 15; ($\bigcirc$) 20; ($\blacksquare$) 0; ($\blacklozenge$) 50; ($\blacktriangle$) 100; ($\bullet$) 200 s. Fitted curves are empirical, of the form $h = h_0 + a_2 r^2 + a_6 r^6$. Data for a similar set of curves for 0.23 mol m^{-3} sodium chloride solution are given in Appendix 2.

ness can be predicted from double-layer theory [16]. The fringe order is thus known precisely at this thickness, and the order of the interference fringes during drainage can be determined by counting back. Films on hydrophobic surfaces, in contrast, always rupture, making it impossible to ascertain the fringe order in the above manner.

Near the centre of the draining film, where the film is relatively thick and the short range surface forces should bear little effect, there is no appreciable difference between the thinning rates on hydrophilic and hydrophobic surfaces (Fig. 5 a–c). At the boundary (i.e., at the thinnest part of the film) thinning is faster in the film on the hydrophobic surface than that on the hydrophilic surface.

The more rapid thinning of very thin films on the hydrophobic surface can be attributed to either a reduction in electrical double-layer repulsion between the two surfaces [14], or to a relatively long range hydrophobic attraction between the two interfaces [24].

The range at which this difference in surface interaction is first noticeable is difficult to determine directly because of the uncertainty (described above) in the absolute film thickness on hydrophobic surfaces. From Fig. 5, however, we note that the thinning rate at which the behaviour of films on the two different surfaces first diverges corresponds to an appreciable film thickness on a hydrophilic surface. If one assumes that the films on the two surfaces behave identically at large separation (as may be the case in view of the similar thinning rates) then the effect of surface forces on film thinning are also appreciable over significant distances. Certainly, hydrophobic forces appear to
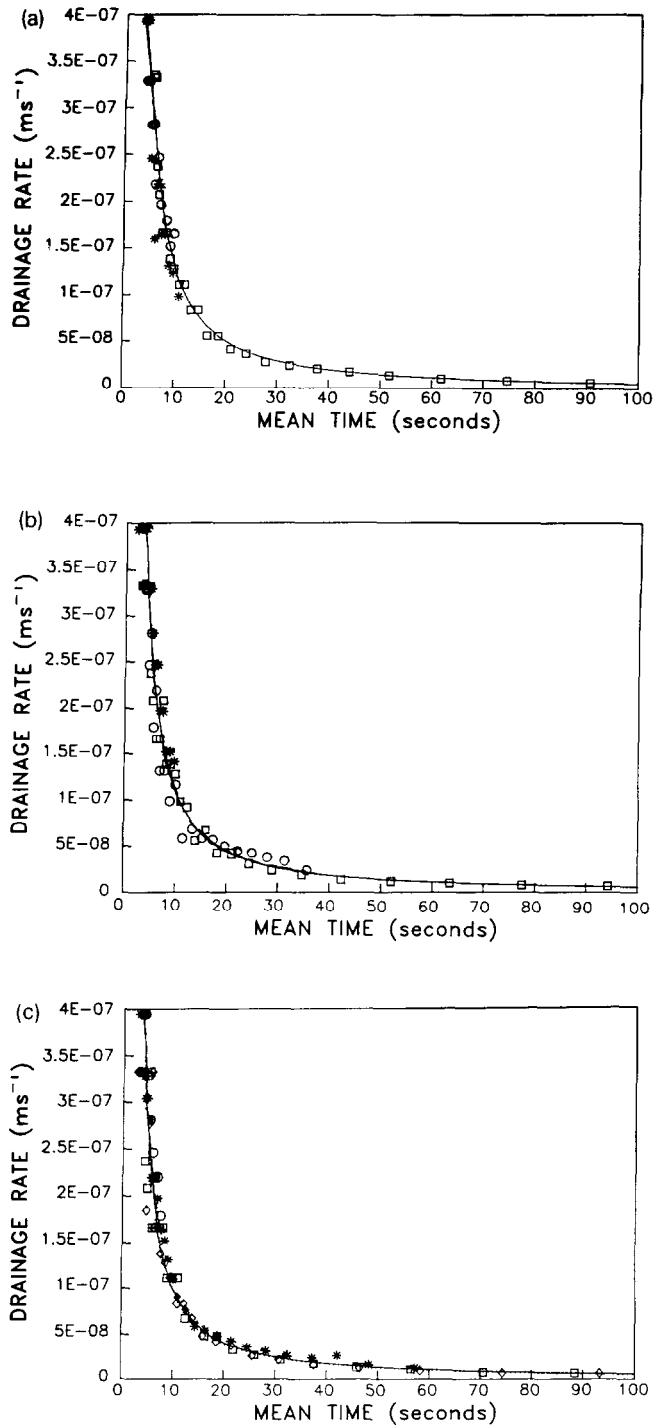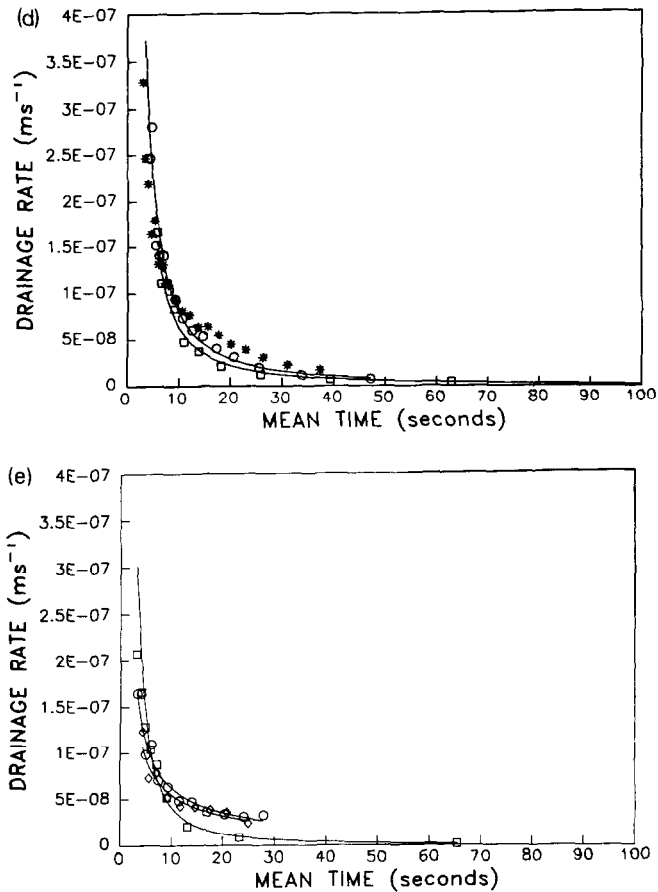
(a)

(b)

(c)

Fig. 5. a, b, c.

Fig. 5. Drainage rate as a function of time for aqueous films (conductivity, $1.2 \cdot 10^{-4}$ S m^{-1}) at hydrophobic and hydrophilic quartz surfaces: ($\square$) hydrophilic; ($\bigcirc$) hydrophobic, contact angle $10 \pm 5°$; ($*$) hydrophobic, contact angle $20 \pm 3°$. (a) Drainage of film centre; (b) $r = 0.05$; (c) $r = 0.10$; (d) $r = 0.25$; (e) $r = 0.30$ mm from the film centre.

extend over distances of 90 nm [24]; however, their precise role in our present system necessitates further work.

ACKNOWLEDGEMENTS

APPENDIX 1

The thinning of a thin aqueous film between a solid plane and an air bubble

Radial symmetry about the z axis is assumed so the film thickness $h = h(r,t)$ is a function only of radial position r and time t. If the film is very thin with respect to characteristic radii, derivatives of h with respect to r are much smaller than unity, velocities are purely radial and the pressure P in the film is a function of radius only.

For slow thinning the inertia of the fluid is neglected. Setting to zero the forces acting on a small volume element relates P to the shear stress Λ:

$$\frac{\partial \Lambda}{\partial z} = \frac{\partial P}{\partial r}$$

For laminar flow the viscosity η of the film relates the velocity gradient to the shear stress:

$$\frac{\partial V}{\partial z} = \frac{\Lambda}{\eta}$$

The film layer in contact with the solid is stationary and, in the absence of surfactants, the layer in contact with the air has a zero shear. This gives a parabolic velocity profile and the average (radial) velocity $\bar{V}(r)$ is given by:

$$\bar{V}(r) = \frac{-h^2}{3\eta} \frac{\partial P}{\partial r}$$

The equation of continuity relates the rate of thinning to the average velocity:

$$\frac{\partial h}{\partial t} = -\bar{V}\frac{\partial h}{\partial r} - \bar{V}\frac{h}{r} - h\frac{\partial \bar{V}}{\partial r}$$

whence

$$\frac{\partial h}{\partial t} = \frac{h^2}{3\eta}\left(h\frac{\partial^2 P}{\partial r^2} + 3\frac{\partial h}{\partial r}\frac{\partial P}{\partial r} + \frac{h}{r}\frac{\partial P}{\partial r} \right)$$

One component of the pressure is the Young–Laplace pressure γC where γ is

the tension of the air–film interface and C is the curvature of that interface. With the approximation that $\dfrac{\partial h}{\partial r} \ll 1$, the curvature of this surface of revolution is:

$$C = \frac{\partial^2 h}{\partial r^2} + \frac{1}{r}\frac{\partial h}{\partial r}$$

The interaction of the two interfaces produces a force per unit area, F:

$$P = -\gamma C - F + P_{\text{bubble}}$$

Substitution into the expression given above for the local thinning rate gives an equation relating h, r and t:

$$\frac{\partial h}{\partial t} = -\frac{h^2\gamma}{3\eta}\left[h\frac{\partial^4 h}{\partial r^4} + \left(\frac{2h}{r} + 3\frac{\partial h}{\partial r}\right)\frac{\partial^3 h}{\partial r^3} + \left(-\frac{h}{r^2} + \frac{3}{r}\frac{\partial h}{\partial r}\right)\frac{\partial^2 h}{\partial r^2} \right.$$
$$\left. + \left(\frac{h}{r^3} - \frac{3}{r^2}\frac{\partial h}{\partial r}\right)\frac{\partial h}{\partial r}\right] - \frac{h^2}{3\eta}\left[h\frac{\partial^2 h}{\partial r^2}\frac{\partial F}{\partial h} + \left(\frac{\partial h}{\partial r}\right)^2\left(h\frac{\partial^2 F}{\partial h^2} + 3\frac{\partial F}{\partial h}\right) + \frac{h}{r}\frac{\partial h}{\partial r}\frac{\partial F}{\partial h}\right]$$

This equation, which has been presented without the physical derivation by Buevich and Lipkina [13,17], cannot be solved analytically, and numerical solutions of the general case are exceedingly awkward because of the high order derivatives. Specific cases have been solved [13,18–20] but comparison with experiment is unhelpful because of the sensitive dependence on initial conditions. Approximate methods [15,21–23] have also been used in attempts to model film thinning. To facilitate comparison with such analyses, we have fitted empirical curves (polynomials of the form $a_0 + a_2 r^2 + a_6 r^6$) to the data. In Appendix 2 we tabulate the important parameters of such fits for different times. h_0 is the axial thickness, $-a_2$ is the coefficient of the quadratic term and yields the curvature and thus the Laplace pressure at the origin, h_b is the thickness.

APPENDIX 2

Empirical polynomial fits to the profile $h(r)$ were made for a range of times t for the film of 0.23 mol m^{-3} sodium chloride solution. The linear term of such a polynomial must be zero so the leading coefficients are the constant h_0 (the thickness at the centre) and the quadratic coefficient a_2.

These are given in Table 1. Also in Table 1 is the value of the minimum thickness h_b of the boundary ring, as obtained from the best fit. All distances are given in μm. Three figures are given to minimise round-off errors, but it is not implied that all are significant.

TABLE 1

Empirical polynomial fits to the profile $h(r)$ for a range of times

Time (s)	h_0 (μm^{-1})	$a_2 \cdot 10^5$ (μm^{-1})	h_b (μm^{-1})
2	3.70	-3.86	1.069
3	3.28	-3.57	0.849
4	3.01	-3.33	0.734
5	2.81	-3.26	0.583
10	2.18	-2.80	0.267
15	1.86	-2.42	0.210
20	1.63	-2.15	0.162
30	1.37	-1.82	0.126
50	1.10	-1.45	0.108
100	0.78	-1.13	$-$
200	0.47	-0.65	0.027

REFERENCES

1   J. Ralston, Adv. Colloid Interface Sci., 19 (1983) 26.
2   L.R. Fisher and N.S. Parker in E. Dickinson and G. Stainsby (Eds), Advances in Food Emulsions and Foams, Elsevier Applied Science, Barking, 1988, p. 45.
3   D.S. Dimitrov, Prog. Surf. Sci., 14 (1983) 295.
4   B.V. Derjaguin and M. Kussakov, Acta Physicochem. URSS, 10 (1939) 25.
5   G.A.H. Elton, Proc. R. Soc. London Ser. A, 194 (1948) 275.
6   D.J. Platikanov, Phys. Chem., 68 (1964) 3619.
7   L.R. Fisher, N.S. Parker and F. Sharples, Opt. Eng., 19 (1980) 798.
8   J. Requena, D.E. Brooks and D.A. Haydon, J. Colloid Interface Sci., 60 (1977) 38.
9   L.R. Fisher and N.S. Parker, Biophys. J., 46 (1984) 253.
10   L.R. Fisher, N.S. Parker and D.A. Haydon, R. Soc. Chem. Faraday Discuss., 81 (1986) 249.
11   L.R. Fisher, E.E. Mitchell and N.S. Parker, in E. Dickinson (Ed.), Food Emulsions and Foams, R. Soc. Chem. London, 1987, p. 230.
12   B. Yavorsky and A. Detlaf, Handbook of Physics, MIR Publishers, Moscow, 1980, p. 793.
13   Yu.A. Buevich and E.Kh. Lipkina, Colloid J. USSR, 40 (1978) 167, English translation.
14   R.M. Pashley and J.A. Kitchener, J. Colloid Interface Sci., 71 (1979) 491.
15   S. Hartland and J.D.J. Robinson, Colloid Interface Sci., 60 (1977) 72.
16   R.J. Hunter, Foundations of Colloid Science, Vol. 1, Clarendon Press, Oxford, 1987.
17   Yu.A. Buevich and E.Kh. Lipkina, J. Appl. Mech. Tech. Phys., 2 (1975) 217, English translation.
18   C.-Y. Lin and J.C. Slattery, AIChE J., 28 (1982) 147.
19   J.D. Chen and J.C. Slattery, AIChE J., 28 (1982) 955; 29 (1983) 174; 256.
20   J.-D. Chen, J. Colloid Interface Sci., 98 (1984) 329.
21   S.P. Frankel and K.J. Mysels, J. Phys. Chem., 66 (1962) 190.
22   D.S. Dimitrov and I.B. Ivanov, J. Colloid Interface Sci., 64 (1978) 97.
23   R.K. Jain and I.B. Ivanov, J. Chem. Soc. Faraday Trans. 2, 76 (1980) 250.
24   H.K. Christenson, P.M. Claesson, J. Berg and P.C. Herder, J. Phys. Chem., 93 (1989) 1472.